Journal Name

RSCPublishing

ARTICLE

Understanding the adsorption mechanism of noble gases Kr and Xe in CPO-27-Ni, CPO-27-Mg, and ZIF-8

Cite this: DOI: 10.1039/xoxxoooooox

O.V. Magdysyuk,[a]* F. Adams,[a] H-P. Liermann,[b] I. Spanopoulos,[c] P.N. Trikalitis,[c] M. Hirscher,[d] R.E. Morris,[e] M.J. Duncan,[e] L.J. McCormick,[e] R.E. Dinnebier,[a]*

Received ooth July 2014,
Accepted ooth January 2014

DOI: 10.1039/xoxxoooooox

www.rsc.org/

An experimental study of Xe and Kr adsorption in metal-organic frameworks CPO-27-Ni, CPO-27-Mg, and ZIF-8 was carried out. *In situ* synchrotron X-ray powder diffraction experiments allowed precise determination of the adsorption sites and sequence of their filling with increasing of gas pressure at different temperatures. Structural investigations were used for interpretation of gas adsorption measurements.

Introduction

Noble gases play a significant role in many industrial and medical applications, but their practical using is restricted by high cost of noble gas separation due to the lack of chemical reactivity and very low boiling/melting points. A mixture of krypton and xenon is obtained by energetically intensive cryogenic distillation of air, which initially contains only 1.14 ppm of krypton and 0.087 ppm of xenon. This mixture can be further separated either by cryogenic distillation or, less expensively, by molecular sieves of nanoporous materials such as zeolites, metal-organic frameworks (MOFs), or activated carbon. Thus, the development of new porous materials (zeolites and MOFs) for adsorption-based separation of noble gases is critically important for their industrial applications. MOFs have several advantages as compared to zeolites: cheaper and simpler synthesis, high diversity of pore structures, and numerous possibilities for postsynthetic modifications.

Despite the importance of MOFs for noble gas storage and separation, only a few studies of krypton and xenon adsorption are reported to date[1-12] and only three studies of adsorption sites of noble gases in MOFs by means of X-ray or neutron diffraction,[13-15] despite the fact that the major adsorption sites and their binding energies are the key features of a material that determines its adsorption properties at a given temperature and pressure, and their identification is a basis for further modifications of the crystal structure of the MOF in order to achieve maximal storage capacity and selectivity. The study of noble gas adsorption in HKUST-1[15] revealed that the interaction of noble gases with MOFs can be completely different from the adsorption of other atoms and molecules like D_2, C_2H_2, CO_2, or CH_4 (methane is a nonpolar gas whose diameter and polarizability are similar to those of Kr). These molecules bind to the open metal sites, [16-19] while structural investigations did not show any evidence of the binding of noble gases Ne, Ar, Kr, and Xe to the open metal sites.[15]

The metal-organic framework CPO-27 (MOF-74) was first synthesized in 2005[20] and is still one of the most interesting MOFs due to several unique characteristics: highest concentration of open metal sites reported to date for MOFs,[21] very high surface area, and uniform 1D channels. Another attractive property of CPO-27 is the existence of a series of isostructural MOFs obtained by replacement of the metal atom, thus providing the unique possibility to investigate the influence of different metal ions (M = Zn, Co, Ni, Mg, Mn, Fe, Cu, Zn/Co, Mg/Ni, Cd) for adsorption properties,[20-30] as well as the possibility to expand the pore apertures of CPO-27 to an isoreticular series with pore apertures ranging from 14 Å to 98 Å,[31] and diverse possibilities for postsynthetic functionalization.[5,32-33]

CPO-27 is composed of M^{II} ions generating linear, infinite-rod secondary building units (SBUs) bound by 2,5-dioxido-1,4-benzenedicarboxylate (DOBDC) ligands, resulting in a hexagonal, 1D pore structure (Fig. 2). Water molecules complete the coordination sphere of the M^{II} ions (5 oxygen atoms from the DOBDC ligand and one oxygen atom from water molecule) and fill the pores. The water molecules are removed upon heating and/or evacuation in order to generate coordinatively unsaturated metal sites.[23,34] The activated material has a characteristic honeycomb structure composed of 1D channels with abundant open metal sites. The open metal sites were found to be preferable for the adsorption of many gases in CPO-27: O_2 and N_2 in CPO-27-Fe,[26] CO_2 in CPO-27-Ni [35] and CPO-27-Mg,[19] CH_4 in CPO-27-Mg,[36] H_2S molecule in CPO-27-Ni,[37-38] and C_2H_2 in CPO-27-Co,[39] C_2H_2, C_2H_4, C_2H_6, C_3H_6, and C_3H_8 in CPO-27-Fe.[40]

ZIF-8 belongs to the class of zeolitic imidazolate frameworks (ZIFs). It consists of tetrahedral units of ZnN_4 linked by 2-methilimidazolate ligands, forming a sodalite-type structure.[41-42] Nanopores are accessible only through narrow channels, and even adsorption of small H_2 molecules was not expected.[43] Recent investigations showed that ZIF-8 can adsorb even C_4 hydrocarbon molecules with an effective diameter size of 5.0 Å, although their diffusivity is 14 orders of magnitude lower than for He (2.6 Å).[44] The effective aperture size of ZIF-8 for molecular sieving was estimated to be in the range of 4.0 to 4.2 Å, which is significantly larger than the XRD-derived value of 3.4 Å, and can be applied for the separation of C_3 and C_4 hydrocarbon mixtures, including mixtures of the corresponding isomers.[44] The explanation of this effect was recently suggested[45] and associated with the gate opening effect, which is initiated by ligand distortion: methyl imidazolate ligands of ZIF-8 show a swing effect upon gas adsorption; thus the pores open and give access to the cavity. Other attractive properties of ZIF-8 include exceptional chemical and thermal stability.

Two important parameters determine the adsorption capacity and selectivity of MOFs: channel morphology and polarizability effects

of adsorption sites (which determine the magnitude of Van der Waals interaction between noble gas atoms and framework). Recent Monte Carlo simulations on 137000 hypothetical MOFs have shown that structures with uniform 1D tube-like channels with diameter of pores large enough to fit a single Xe atoms can be ideal materials for Xe-Kr separation.[46] A recent detailed theoretical study revealed that CPO-27 is one of few promising MOFs for noble gas storage and separation due to its relatively high selectivity, gas permeability, and working capacity.[47-48] Nevertheless, the origin of gas selectivity and the effect of different metal ions on the noble gas adsorption ability of CPO-27 are still unclear. Recently, large selectivity of ZIF-8 for Xe/Kr separation was predicted from single adsorption isotherm measurements, with a ratio of ~ 8 at low pressure, decreasing to ~ 5.5 at a pressure above 1000 mbar.[49-50] Isosteric heat of adsorption of 20 KJ/mol for Xe and of 14 KJ/mol for Kr was reported, remaining almost constant upon gas loading up to a pressure of 1000 mbar.[50]
In order to get deeper insight into the mechanism of gas loading by CPO-27 and ZIF-8, we examined the temperature-dependent uptake of Xe and Kr by CPO-27 with abundant open metal sites (for Ni and Mg) along uniform channels, and ZIF-8 without accessible open metal sites. A rigorous study of the adsorption properties via X-ray powder diffraction scattering methods and thermal adsorption spectroscopy on these MOFs provide a detailed description of the loading characteristics, which are critical for the design of next-generation materials.

Experimental

Synthesis

CPO-27-Ni [23] and CPO-27-Mg [51] were prepared using literature methods. Sample ZIF-8 was provided by BASF as Basolite Z-1200.

X-ray powder diffraction measurements

Synchrotron X-ray powder diffraction measurements of CPO-27-Ni (Xe and Kr adsorption), and CPO-27-Mg (Xe adsorption) were performed at the High-Resolution Powder Diffraction beamline P02.1 of PETRA III (λ = 0.20727 Å). Synchrotron X-ray powder diffraction measurements of CPO-27-Mg (Kr adsorption) and ZIF-8 (Xe and Kr adsorption) were performed at the High-Resolution Powder Diffraction beamline ID31 of ESRF (λ = 0.4 Å). All samples were loaded in quartz capillaries, activated *in situ* at 453 K for 2-3 hours before gas loading, and validated by Rietveld refinement. Then they were cooled down to room temperature and exposed to Kr or Xe gas. Before changing the gas pressure, samples were heated 30 K above the measurement's temperature. X-ray powder diffraction measurements of Xe and Kr adsorption in ZIF-8 were performed at 180 K at different pressures. Samples were evacuated at 433 K for 3 hours before gas loading, and their structure was validated by Rietveld refinement. Then they were cooled to room temperature and exposed to Kr or Xe gas. Before changing gas pressure, samples were always heated to room temperature. All diffraction data were analysed by the Rietveld method, simulated annealing and difference Fourier synthesis as implemented in the program TOPAS 4.1.[52] The global optimization method of simulated annealing was used to determine the positions of the missing noble gas atoms, which were subsequently refined by Rietveld refinement. The final crystal structure was confirmed by difference Fourier analysis.

Adsorption measurements

Structural investigations of the adsorption process of noble gases in CPO-27 were supported by gas adsorption measurements and determination of isosteric heat of adsorption. Experimental heats of adsorption curves were determined from measured gas adsorption isotherms up to 1 bar at temperatures 180 K, 200 K, and 220 K for Kr and 240 K, 260 K and 280 K for Xe, by applying a virial type equation (Fig. 1).

The reported value of heat of adsorption of ZIF-8 is 20(1) kJ/mol for Xe and 14(1) kJ/mol for Kr at low loadings and remains almost unchanged or slightly increasing over the measured pressure range.[50]

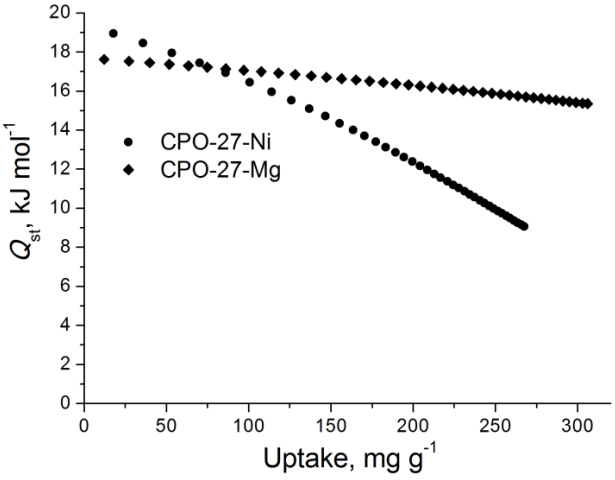

Figure 1a. Isosteric heat of Kr adsorption for CPO-27-Ni and CPO-27-Mg.

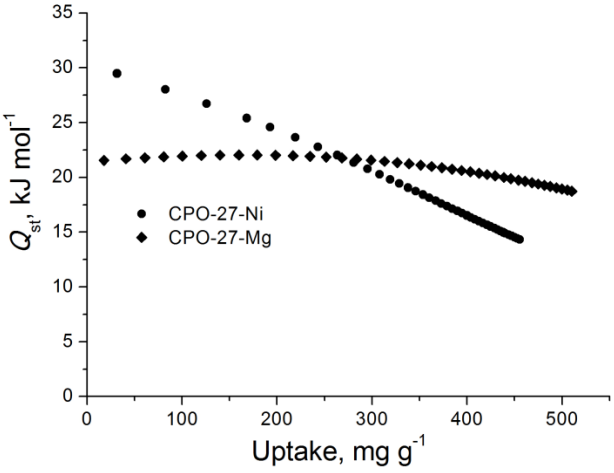

Figure 1b. Isosteric heat of Xe adsorption for CPO-27-Ni and CPO-27-Mg.

Results and Discussion

I. Structural investigation of Kr and Xe adsorption in CPO-27-Ni and CPO-27-Mg.

Rietveld refinements of CPO-27-Ni and CPO-27-Mg loaded with Kr and Xe revealed that the preferable adsorption positions for Kr are similar to those of Xe in the corresponding MOF with only slight differences in the refined positions (Fig. 2).

The crystal structure of CPO-27-Ni determined for low loading of Xe and Kr confirms that the vacant coordination sites on the metal ions are the strongest adsorption sites with a Ni-Xe distance of 3.01(2) Å and a Ni-Kr distance of 3.03(3) Å at 1000 mbar. The second adsorption site appears almost simultaneously with the first adsorption site, having approximately half the occupancy of the first adsorption site at all measured temperatures. It is located at a distance of 4.10(3) Å from the carboxylate oxygen atom and at 4.23(3) Å from the phenolic oxygen (170K, 1000 mbar) for Xe, and at a distance of 4.02(3) Å from the carboxylate oxygen and 4.10(3) Å from the phenolic oxygen atoms of the ligand (130K, 1000 mbar) for Kr. The distance between first and second adsorption sites is ~3.5 Å, so only one of two adsorption sites can be occupied. The third

adsorption site for both, Xe and Kr atoms, is located in the center of the channels and represents unbounded noble gas atoms due to the diffusion barriers.[53]

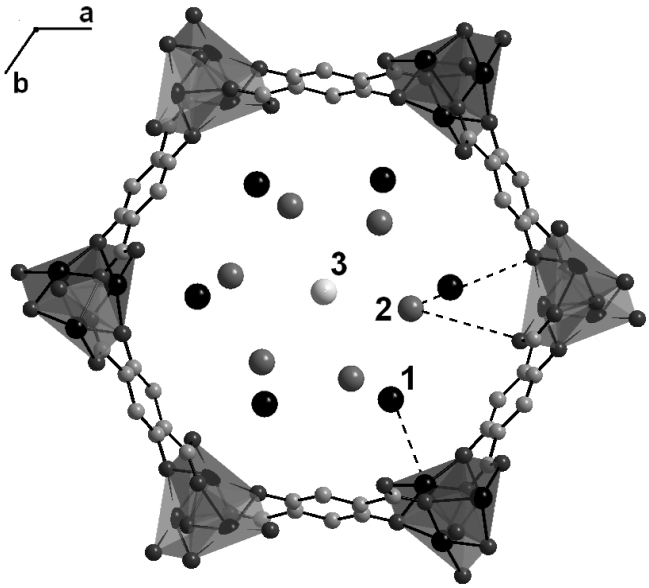

Figure 2. Projection of the 1D channels of CPO-27 along the *c*-axis showing adsorbed Kr and Xe atoms. The numbers denote crystallographically independent positions of Kr and Xe atoms (numbers 1, 2, and 3). Framework atoms: grey polyhedra – NiO_5 or MgO_5, grey spheres – carbon.

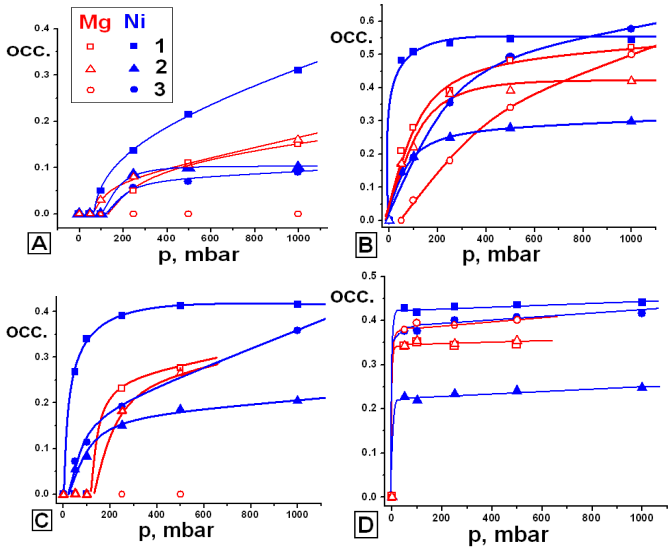

Figure 3. Fractional occupancies of the three atomic positions for Kr and Xe in CPO-27-Ni (blue symbols) and CPO-27-Mg (red symbols), where 1 – coordinates open metal sites, 2 – coordinates oxygen atoms, 3 – located in the center of channel. (A) Kr adsorption at 250K; (B) Kr adsorption at 170K; (C) Xe adsorption at 250K; (D) Xe adsorption at 170K. Multiplicity of positions no.1 and no.2 is 18, multiplicity of position no.3 is 3. Lines – guides for the eyes.

Unexpected Xe and Kr adsorption behavior was found for CPO-27-Mg. In this case the second binding site near the oxygen atoms is almost simultaneously occupied with the first binding site near the open metal ion and has a similar value of the fractional occupancy. The Mg-Xe distance is 3.14(2) Å at 170K (500 mbar), and the Mg-Kr distance is 3.23(3) Å at 130K (1000 mbar). The second adsorption site for Xe is at a distance of 4.10(3) Å from the carboxylate oxygen atom at a distance of 4.23(3) Å from the phenolic oxygen atom (170K, 500 mbar). The second adsorption site for Kr is at 3.92(3) Å from the carboxylate oxygen group and 3.96(3) Å from the phenolic oxygen atom (130K, 1000 mbar). The third adsorption site for both, Xe and Kr, is located in the center of the channel, and its occupancy is highest at lowest temperatures and is decreasing with increasing temperature. At 250K the third adsorption site is unoccupied since the first and the second strong adsorption sites are not fully occupied at this temperature (Fig. 3).

As a result, CPO-27-Mg shows weaker binding to both Xe and Ke atoms than CPO-27-Ni. This may be explained by the larger polarizability of the Ni atom in comparison to the Mg atom. In contrast to noble gas adsorption, the adsorption of deuterated methane in CPO-27-Mg revealed much stronger binding of the CD_4 molecule to open metal sites than to the second adsorption site near oxygen atoms, because the second adsorption site is filled only after the first adsorption site.[36]

The experimental results for CPO-27 revealed that the open metal sites are the major (in the case of Ni^{2+}) or one of two major (in the case of Mg^{2+}) binding sites for Xe and Kr gases. On the other hand, a recent report of noble gas adsorption in HKUST-1 did not show any interaction of noble gas atoms with open Cu^{2+} metal sites.[15] Thus, noble gas adsorption behaviour depends not only on the presence of the open metal sites, but also on the pore's topology. The small pockets in HKUST-1 provide strong geometrical confinement of noble gas atoms, while the uniform channels of CPO-27 do not impose geometrical restrictions on noble gas adsorption, and the more easily polarizable sites along the channels are therefore the main adsorption sites.

For the noble gas atoms, the adsorption depends on the polarizability of the framework. The polarizability of Xe atoms exceeds the polarizability of Kr atoms, and polarizable metal ions enhance the interaction with noble gas atoms. This effect is responsible for noble gas adsorption in CPO-27-Ni. On the other hand, CPO-27-Mg possesses a highly ionic Mg-O bond,[24] causing two strong adsorption sites along it: open Mg atoms and corresponding oxygen atoms, providing a more homogeneous distribution of adsorption sites along the channels. In previous works, sites near the metal centres were found to be the major adsorption sites in Zn-MOF-5[13] and Zn-MFU-4*l*,[14] but not in Cu^{II}-HKUST-1,[15] showing strong specific interaction of the noble gas atoms with metal atoms.

The measured heat of adsorption of CPO-27-Mg is 18(1) kJ/mol for Kr and 22(1) kJ/mol for Xe at low loadings and remains almost unchanged over the measured pressure range (Fig. 1). The measured heat of adsorption of CPO-27-Ni is 19(1) kJ/mol for Kr and 30(1) kJ/mol for Xe at low loadings, and drops nearly by a factor of 2 with increasing loading (Figs 1), indicating strong interaction between open metal sites and adsorbed atoms. The small variations of isosteric heats of adsorption for CPO-27-Mg during Kr and Xe adsorption indicates a homogeneous distribution of adsorption sites along the channels and is fully consistent with the presence of two major adsorption sites with a very similar binding strength: open metal sites Mg^{2+} and carboxylate oxygen atoms. A similar effect was observed for isosteric heat of adsorption of Ar, Kr, and Xe in porous $Co_3(HCOO)_6$:[11] accessible but not abundant metal sites and oxygen atoms from C=O bonds are homogeneously distributed along the channels, and the isosteric heat of adsorption of noble gases remains almost constant. CPO-27-Ni shows a more heterogeneous distribution of adsorption sites along the channels – the open metal sites provide stronger binding of noble gas atoms than the sites close to the oxygen atoms, and this is reflected in a strong variation of

isosteric heat of adsorption as a function of loading, when filling of available open metal sites leads to a decrease of isosteric heat of adsorption. The experimental results indicate that CPO-27-Ni possesses better selectivity in Xe/Kr separation than CPO-27-Mg.

The reported isosteric heat of adsorption of CH_4 is 18(1) kJ/mol for CPO-27-Mg and 19(1) kJ/mol for CPO-27-Ni and remains almost unchanged with increasing loading.[54] This allows some speculations, that both CPO-27-Mg and CPO-27-Ni can have two main adsorption sites of similar strength for methane molecules – open metal sites and sites close to oxygen atoms. There is also a possibility of strong attractive interaction between adsorbed CH_4 molecules, which can compensate for the decrease of the isosteric heat of adsorption due to heterogeneous distribution of the adsorption sites. The structural investigations of CH_4 adsorption in CPO-27 would allow comparison of the adsorption process of noble gases and methane in these MOFs. The isosteric heat of adsorption of hydrogen is slightly higher for CPO-27-Ni then for CPO-27-Mg, and remains constant until ca. one hydrogen molecule per metal atom is adsorbed,[55] and the corresponding metal-H_2 distances are shorter for CPO-27-Ni,[25] thus, the binding energy of H_2 at the nickel open metal site is stronger in comparison to the magnesium open metal site.

II. Adsorption of Kr and Xe in ZIF-8.

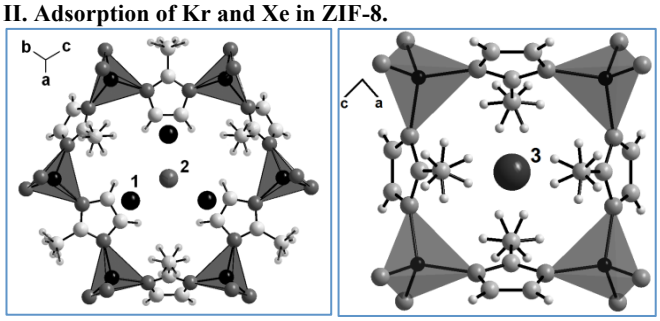

Figure 4. Positions of noble gas atoms (numbers 1, 2, 3) in cavities of ZIF-8 (fourth position in the center of cavity is not shown). Framework atoms: grey tetrahedra of ZnN_4, large white spheres – carbon atoms, small white spheres – hydrogen atoms.

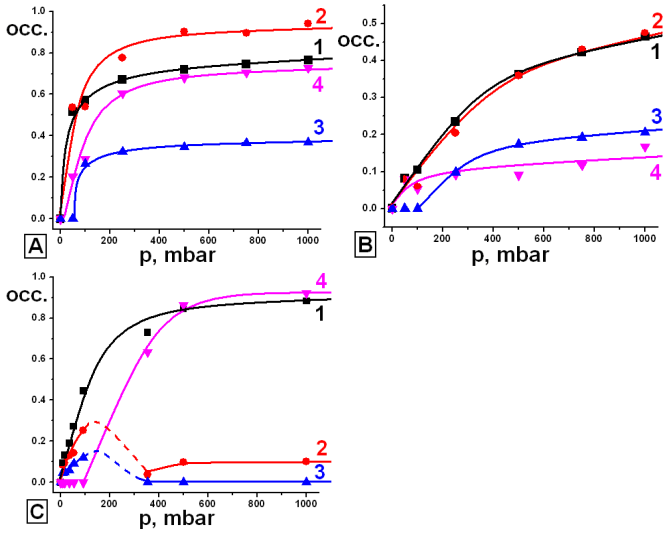

Figure 5. Fractional occupancies of all atomic positions for Kr and Xe in ZIF-8, where position 1 – coordinates C=C bond of imidazolate, position 2 – coordinates center of 6-membered window, position 3 – coordinates 4-membered window, position 4 – coordinates center of cavity. (A) Kr adsorption at 130K, position in 4-membered window is split; (B) Kr adsorption at 180K; (C) Xe adsorption at 180K. Multiplicity of positions no.1 is 24, no.2 is 8, no.3 is 24 for Kr and 12 for Xe, and no. 4 is 2. Lines – guides for the eyes.

Structural investigation of Xe and Kr adsorption by ZIF-8 demonstrates the important role of the gate opening effect, which is responsible for the strong increase of noble gas adsorption.

The main adsorption site for both Kr and Xe atoms was found near the imidazolate ligand, similar to the first adsorption site for a D_2 molecule,[43] in contrast to CPO-27, where the main adsorption sites were identified as the open metal atoms and/or the highly polarizable C=O bond. Metal sites in ZIF-8 are not accessible even for the small D_2 molecules due to steric hindrance by surrounding ligands,[56] and there are no highly polarizable carbon-oxygen bonds in the ZIF-8 structure. The most polarizable bond remaining accessible for adsorbed noble gas atoms in ZIF-8 is the C=C double bond of the imidazolate ligand. Thus, this adsorption site with multiplicity 24 is the first filling site during noble gas adsorption and has the highest fractional occupancy. The second adsorption site with multiplicity 8 is located at the center of 6-membered windows and corresponds to the position of the third adsorption site of D_2.[43] The sequence of filling of the adsorption sites and their localization are different for Xe and for Kr atoms due to large differences in their atomic radii and polarizabilty, as well as due to the geometrical factor of the relatively small pore volume of ZIF-8.

At very low pressure of 9 mbar Xe atoms occupy three crystallographically different positions (Fig. 4): near the C=C bond of the imidazolate (at a distance of ~ 4 Å from the carbon atom in C=C bond), the center of 6-membered ZnN_4 windows (at a distance of ~ 4 Å from the carbon atom in C=C bond), and within the 4-membered windows (corresponds to the fourth adsorption site for D_2 molecule.[43] Between 93 mbar and 394 mbar the gate opening effect was observed, and the forth position in the center of the pore is occupied (this position was not observed for D_2 adsorption). Simultaneously, the occupancy of the third position in the 4-membered ZnN_4 windows dropped to zero, and the occupancy of the second position decreased. Further increasing of pressure to 1000 mbar results only in slight increase to the occupancies of all three Xe positions (Fig. 5). The maximum amount of adsorbed Xe atoms at 180K by ZIF-8 corresponds to 2 Xe atoms per Zn atom.

The gate opening was previously observed also for CO and N_2 loading in ZIF-8.[57] In general, the gate opening effect appears when the gas pressure becomes high enough to promote the expansion of the crystal structure through its deformation, resulting in a reorganization of the adsorbed atoms. The deformation of the crystal structure allows a considerable increase of the amount of adsorbed gas. The gate opening effect was not directly observed during Kr adsorption in ZIF-8 at 180K, but its presence can be postulated based on the filling of some adsorption sites inside the cavities exclusively on higher pressure. The sequence of filling of the adsorption sites by Kr is different from Xe adsorption. Three positions were occupied by Kr at 50 mbar and 100 mbar at 180K: near C=C bond of imidazolate (at a distance of ~ 4.1 Å from the carbon atom in C=C bond), the center of 6-membered windows (at a distance of ~ 3.8 Å from the carbon atom in C=C bond), and the center of the cavity (Fig. 4), *i.e.* sites 1, 2 and 4. Increasing pressure to 250 mbar results in the formation of a fourth position in the 4-membered windows, which is split and located at a distance of ~ 4.1 Å to the nearest carbon atom of the C=C bond. The sequence of filling of the adsorption sites by Kr at 130K is similar to that at 180 K. The maximal amount of adsorbed Kr atoms at 130K by ZIF-8 corresponds to 3 Kr atoms per Zn atom (Fig. 5). For comparison, the maximal uptake of methane CD_4 molecules was found to be 3 CD_4 molecules per Zn atom.[58] Also the experimentally determined positions for both Kr and Xe atoms correlate well with theoretically

simulated positions for Ar atoms,[59] and results of grand canonical Monte Carlo simulations.[12]

The adsorption of noble gases by MOFs is based on the polarizability of both possible adsorption sites of the MOF and the adsorbed noble gases. All adsorption sites in ZIF-8 have a relatively low polarizability, although some of them are slightly more polarizable (*i.e.* C=C bond of imidazolate ligand). This fact is also confirmed by isosteric heat of adsorption measurements, which showed no decrease in the isosteric heat of adsorption upon Kr and Xe loading.[50] Thermal desorption measurements showed one broad peak at low loading, which is split into a few peaks with increasing gas loading.[8] Splitting of the desorption peaks can be explained only by the gate opening effect due to the absence of strong adsorption sites (*i.e.* sites with binding strength similar to open metal sites). Thus, the geometrical factor of pore size and shape is the main driving force of noble gas storage and separation in ZIF-8.

Conclusions

A systematic structural investigation of Kr and Xe adsorption sites in different types of MOFs allows the correlation between the crystal structure of a MOF and its ability to adsorb, store and separate noble gases to be drawn. Investigation of noble gas adsorption in CPO-27-Ni, CPO-27-Mg, and ZIF-8 revealed that two main factors influence noble gas adsorption by these MOFs: channel morphology and polarizability of adsorption sites. It could be unambiguously confirmed that open metal sites are the primary and strongest adsorption sites for noble gases, if there is no strong geometric confinement of guest atoms. This is explained by the nature of noble gas adsorption in MOFs. Since noble gases lack chemical reactivity, the only possible mechanism of adsorption for them is Van der Waals interaction based on the polarizability of the atoms. Metal sites are the most polarizable part of the MOF's structure, and thus they are also the main adsorption sites with highest binding energy to adsorbed noble gas atoms, as was confirmed for CPO-27 (present work), MFU-4*l*,[14,60] and MOF-5.[13] The isosteric heat of adsorption of highly polarizable metal sites can be exceeded only by increased interaction between adsorbed atoms and framework, which might be achieved through the geometrical confinement of adsorbed atoms in small pores, i.e. in the cases of ZIF-8 (present work) and HKUST-1.[15] The polarizability of C=O bonds are usually lower as compared to that of metal sites, and they act as a secondary adsorption site (CPO-27, MOF-5). The less polarizable C=C bond is a major adsorption site for noble gases in ZIF-8 due to the absence of accessible metal sites and carbon-oxygen bonds in the crystal structure. The high isosteric heat of adsorption for noble gases in ZIF-8[50] is provided by the geometrical confinement of noble gases in small pores. Thus, MOFs with small pores and abundant accessible metal sites are promising candidates for noble gas storage and separation.

Acknowledgements

Support with synchrotron measurements at PETRA III, P02.1 (proposal I-20130239) to Dr. M. Hinterstein and Dr. J. Bednarcik (PETRA III, Hamburg, Germany), and with synchrotron measurements at ESRF, ID31 (proposals ch3737, ch3878) to Dr. C. Drathen (ESRF, Grenoble, France), Mr. T. Runcevski, Mr. M. Etter (Max Planck Institute for Solid State Research, Stuttgart, Germany) is gratefully acknowledged.

Notes and references

[a] Max Planck Institute for Solid State Research, Heisenbergstr, 1, D-70569 Stuttgart (Germany), E-mail: O.V.Magdysyuk@gmail.com, R.Dinnebier@fkf.mpg.de
[b] Photon Sciences, DESY, Hamburg (Germany)
[c] Department of Chemistry, University of Crete, Voutes 71003, Heraklion (Greece)
[d] Max Planck Institute for Intelligent Systems Heisenbergstr, 3, D-70569 Stuttgart (Germany)
[e] School of Chemistry, University of St Andrews, North Haugh, St Andrews, Fife, Scotland (UK)

Electronic Supplementary Information (ESI) available: details of Rietveld refinement results for all structures, Kr and Xe sorption measurements and heat of adsorption calculations. See DOI: 10.1039/b000000x/

1 U. Mueller, M. Schubert, F. Teich, H. Puetter, K. Schierle-Arndt, J. Pastre, *J. Mater. Chem.* 2006, **16**, 626–636;
2 D. Farrusseng, C. Daniel, C. Gaudillère, U. Ravon, Y. Schuurman, C. Mirodatos, D. Dubbeldam, H. Frost, R.Q. Snurr, *Langmuir.* 2009, **25**(13), 7383–7388;
3 P.K. Thallapally, J.W. Grate, R.K. Motkuri, *Chem. Commun.* 2012, **48**, 347−349;
4 J. Liu, P.K. Thallapally, D. Strachan, *Langmuir.* 2012, **28**, 11584−11589;
5 J. Liu, D.M. Strachan, P.K. Thallapally, *Chem. Commun.* 2014, **50**, 466−468;
6 S.T. Meek, S.L. Teich-McGoldrick, J.J. Perry IV, J.A. Greathouse, M.D. Allendorf, *J. Phys. Chem. C.* 2012, **116**, 19765−19772;
7 C.A. Fernandez, J. Liu, P.K. Thallapally, D.M. Strachan, *J. Am. Chem. Soc.* 2012, **134**, 9046−9049;
8 A. Soleimani Dorcheh, D. Denysenko, D. Volkmer, W. Donner, M. Hirscher, *Microporous and Mesoporous Materials.* 2012a, **162**, 64–68;
9 Y-S. Bae, B.G. Hauser, Y.J. Colón, J.T. Hupp, O.K. Farha, R.Q. Snurr, *Microporous and Mesoporous Materials.* 2013, **169**, 176–179;
10 K.V. Lawler, Z. Hulvey, P.M. Forster, *Chem. Commun.* 2013, **49**, 10959−10961;
11 H. Wang, K. Yao, Z. Zhang, J. Jagiello, Q. Gong, Y. Han, J. Li, *Chem. Sci.* 2014a, **5**, 620–624;
12 Q. Wang, H. Wang, S. Peng, X. Peng, D. Cao, *Phys. Chem. C.* 2014b, **19**, 10221–10229;
13 J.L.C. Rowsell, E.C. Spencer, J. Eckert, J.A.K. Howard, O.M. Yaghi, *Science,* 2005, **309**, 1350–1354;
14 A. Soleimani Dorcheh, R.E. Dinnebier, A. Kuc, O. Magdysyuk, F. Adams, D. Denysenko, T. Heine, D. Volkmer, W. Donner, M. Hirscher, *Phys. Chem. Chem. Phys.* 2012b, **14**, 12892–12897;
15 Z. Hulvey, K.V. Lawler, Z. Qiao, J. Zhou, D. Fairen-Jimenez, R.Q. Snurr, S.V. Ushakov, A. Navrotsky, C.M. Brown, P.M. Forster, *J. Phys. Chem. C.* 2013, **117**, 20116−20126;
16 V.K. Peterson, Y. Liu, C.M. Brown, C.J. Kepert, *J. Am. Chem. Soc.* 2006, **128**, 15578–15579;
17 S. Xiang, W. Zhou, J.M. Gallegos, Y. Liu, B. Chen, *J. Am. Chem. Soc.* 2009, **131**, 12415–12419;
18 H. Wu, J.M. Simmons, Y. Liu, C.M. Brown, X.-S. Wang, S. Ma, V.K. Peterson, P.D. Southon, C.J. Kepert, H.-C. Zhou, T. Yildirim, W. Zhou, *Chem.—Eur. J.* 2010a, **16**, 5205–5214;
19 H. Wu, J.M. Simmons, G. Srinivas, W. Zhou, T. Yildirim, *J. Phys. Chem. Lett.* 2010b, **1**, 1946–1951;
20 N.L. Rosi, J.; Kim, M. Eddaoudi, B.L. Chen, M. O'Keeffe, O.M. Yaghi, *J. Am. Chem. Soc.* 2005, **127**, 1504−1518;
21 M. Märcz, R.E. Johnsen, P.D.C. Dietzel, H. Fjellvåg, *Microporous and Mesoporous Materials.* 2012, **157**, 62–74;
22 P.D.C. Dietzel, Y. Morita, R. Blom, H. Fjellvåg, *Angew. Chem. Int. Ed.* 2005, **44**, 6354–6358;
23 P.D.C. Dietzel, B. Panella, M. Hirscher, R. Blom, H. Fjellvåg, *Chem. Commun.* 2006, **42**, 959–961;
24 S.R. Caskey, A.G. Wong-Foy, A.J. Matzger, (2008). *J. Am. Chem. Soc.* **130**, 10870–10871;
25 W. Zhou, H. Wu, T. Yildirim, *J. Am. Chem. Soc.* 2008, **130**, 15268–15269;
26 E.D. Bloch, L.J. Murray, W.L. Queen, S. Chavan, S.N. Maximoff, J.P. Bigi, R. Krishna, V.K. Peterson, F. Grandjean, G.J. Long, B. Smit, S. Bordiga, C.M. Brown, J.R. Long, *J. Am. Chem. Soc.* 2011, **133**, 14814–14822;

27 J.A. Botas, G. Calleja, M. Sánchez-Sánchez, M.G. Orcajo, *Int. J. Hydrogen Energy*. 2011, **36**, 10834–10844;
28 R. Sanz, F. Martínez, G. Orcajo, L. Wojtas, D. Briones, *Dalton Trans.* 2013, **42**, 2392–2398;
29 J. Kahr, R.E. Morris, P.A. Wright, *CrystEngComm*. 2013, **15**, 9779−9786;
30 M. Diaz-Garcia, M. Sanchez-Sanchez, *Microporous and Mesoporous Materials*. 2014 **190**, 248–264;
31 H. Deng, S. Grunder, K.E. Cordova, C. Valente, H. Furukawa, M. Hmadeh, F. Gándara, A.C. Whalley, Z. Liu, S. Asahina, H. Kazumori, M. O'Keeffe, O. Terasaki, J.F. Stoddart, O.M. Yaghi, *Science*. 2012, **336**, 1018–1023;
32 Y-S. Bae, J. Liu, C.E. Wilmer, H. Sun, A.N. Dickey, M.B. Kim, A.I. Benin, R.R. Willis, D. Barpaga, M.D. LeVan, R.Q. Snurr, *Chem. Commun.* 2014, **50**, 3296–3298;
33 A.F. Cozzolino, C.K. Brozek, R.D. Palmer, J. Yano, M. Li, M. Dincă, *J. Am. Chem. Soc.* 2014, **136**(9), 3334–3337;
34 P.D.C. Dietzel, R.E. Johnsen, R. Blom, H. Fjellvåg, *Chem. Eur. J.* 2008a, **14**, 2389–2397;
35 P.D.C. Dietzel, R.E. Johnsen, H. Fjellvåg, S. Bordiga, E. Groppo, S. Chavan, R. Blom, *Chem. Commun.* 2008b, **44**, 5125–5127;
36 H. Wu, W. Zhou, T. Yildirim, *J. Am. Chem. Soc.* 2009a, **131**, 4995–5000;
37 S. Chavan, F. Bonino, L. Valenzano, B. Civalleri, C. Lamberti, N. Acerbi, J.H. Cavka, M. Leistner, S. Bordiga, *J. Phys. Chem. C*. 2013, **117**(30), 15615–15622;
38 P.K. Allan, P.S. Wheatley, D. Aldous, M.I. Mohideen, C. Tang, J.A. Hriljac, I.L. Megson, K.W. Chapman, G. De Weireld, S. Vaesen and R.E. Morris, *Dalton Trans*, **2012**, *41*, 4060–4066;
39 S. Xiang, W. Zhou, Z. Zhang, M.A. Green, Y. Liu, B. Chen, *Angew. Chem., Int. Ed.* 2010, **49**, 4615−4618;
40 E.D. Bloch, W.L. Queen, R. Krishna, J.M. Zadrozny, C.M. Brown, J.R. Long, *Science.* 2012, **335**, 1606–1610;
41 X.C. Huang, Y.Y. Lin, J.-P. Zhang, X.M. Chen, *Angew. Chem., Int.Ed.* 2006, **45**, 1557−1559;
42 K.S. Park, Z. Ni, A.P. Cote, J.Y. Choi, R. Huang, F.J. Uribe-Romo, H.K. Chae, M. O'Keefe, O.M. Yaghi, *Proc. Natl. Acad. Sci. U.S.A.* 2006, **103**, 10186–10191;
43 H. Wu, W. Zhou, T. Yildirim, *J. Am. Chem. Soc.* 2007, **129**, 5314–5315;
44 C. Zhang, R.P. Lively, K. Zhang, J.R. Johnson, O. Karvan, W.J. Koros, *J. Phys. Chem. Lett.* 2012, **3**, 2130−2134;
45 D. Fairen-Jimenez, S.A. Moggach, M. T. Wharmby, P.A. Wright, S. Parsons, T. Düren, *J. Am. Chem. Soc.* 2011, **133**, 8900−8902;
46 B.J. Sikora, C.E. Wilmer, M.L. Greenfield, R.Q. Snurr, *Chem. Sci.* 2012, **3**, 2217;
47 Y. Gurdal, S. Keskin, *Ind. Eng. Chem. Res.* 2012, **51**, 7373−7382;
48 Y. Gurdal, S. Keskin, *J. Phys. Chem. C.* 2013, **117**, 5229−5241;
49 P. Ryan, O.K. Farha, L.J. Broadbelt, R.Q. Snurr, (2011). *AIChE J.* **57**, 1759;
50 P.J. Ryan, O.K. Farha, L.J. Broadbelt, R.Q. Snurr, Y-S. Bae, (2014). Patent US 2014/0013943 A1;
51 R.E. Morris, P.S. Wheatley, S.J. Warrender and M.J. Duncan, *Synthesis of MOFs*, WO2013186542A1, 19th Dec 2013;
52 A.A. Coelho, (2007). TOPAS. Version 4.1. Coelho Software, Brisbane, Australia;
53 P. Canepa, N. Nijem, Y.J. Chabal, T. Thonhauser, *Materials. Phys. Rev. Lett.* 2013, **110**, 026102;
54 D. Yu, A.O. Yazaydin, J.R. Lane, P.D.C. Dietzel, R.Q. Snurr, *Chem. Sci.* 2013, **4**, 3544−3556;
55 P.D.C. Dietzel, P.A. Georgiev, Ju. Eckert, R. Blom, Th. Strässle, T. Unruh, *Chem. Commun.* 2010, **46**, 4962–4964;
56 W. Zhou, Q. Wang, L. Zhang, Y-C. Liu, Y. Kang, *J. Phys. Chem. B,* 2009, **113**(32), 11049−11053.
57 C.O. Ania, E. Garcia-Perez, M. Haro, J.J. Gutierrez-Sevillano, T. Valdes-Solis, J.B. Parra, S. Calero, *J. Phys. Chem. Lett.* 2012, **3**, 1159−1164;
58 H. Wu, W. Zhou, T. Yildirim, *J. Phys. Chem. C*, 2009b, **113**, 3029–3035;
59 E. Pantatosaki, F.G. Pazzona, G. Megariotis, G.K. Papadopoulos, *J. Phys. Chem. B.* 2010, **114**, 2493–2503;
60 O.V. Magdysyuk, D. Denysenko, I. Weinrauch, D. Volkmer, M. Hirscher, R.E. Dinnebier, 2014 (*in preparation*)